Drift velocity of edge magnetoplasmons due to magnetic edge channels

Alexey A. Sokolik ⬤* and Yurii E. Lozovik

Laboratory for Spectroscopy of Nanostructures, Institute for Spectroscopy RAS, 108840 Troitsk, Moscow, Russia;
Institute of Microelectronics Technology and High Purity Materials, Russian Academy of Sciences, 142432 Chernogolovka, Russia;
and Faculty of Physics, National Research University Higher School of Economics, 109028 Moscow, Russia

Edge magnetoplasmons arise on a boundary of conducting layers in perpendicular magnetic field due to an interplay of electron cyclotron motion and Coulomb repulsion. Lateral electric field, which confines electrons inside the sample, drives their spiraling motion in magnetic field along the edge with the average drift velocity contributing to the total magnetoplasmon velocity. We revisit this classical picture by developing fully quantum theory of drift velocity starting from analysis of magnetic edge channels and their electrodynamic response. We derive the quantum-mechanical expression for the drift velocity, which arises in our theory as a characteristic of such response and can be calculated as the harmonic mean of group velocities of edge channels crossing the Fermi level. Using the Wiener-Hopf method to analytically solve the edge mode electrodynamic problem, we demonstrate that the edge channel response effectively enhances the bulk Hall response of the conducting layer and thus increases the edge magnetoplasmon velocity. In the long-wavelength limit of our model, the drift velocity is simply added to the total magnetoplasmon velocity, in agreement with the classical picture.

I. INTRODUCTION

Edge magnetoplasmons on a boundary of two-dimensional electron gas (2DEG) are induced jointly by electric field from electron density perturbations near the edge and by Lorentz force from the external magnetic field [1]. Due to the time-reversal symmetry breaking in magnetic field, edge magnetoplasmons propagate along the sample boundary only in one direction and cannot scatter back. This property, together with strong confinement of plasma oscillations near the boundary, is essential to possible applications of edge magnetoplasmons for energy and signal transmission on the micro- and nanoscale [2–5]. Edge magnetoplasmons were studied experimentally on boundaries of 2DEG formed by depleting gate electrodes [6–17], on graphene edges [18–25], and, recently, on the edges of quantum anomalous Hall insulators which do not require external magnetic field to support magnetoplasmons [26–28].

Theoretical treatment of edge magnetoplasmons relies on various approximations applied to solve Maxwell equations for a conducting half-plane [1,29–31] or on the exact Wiener-Hopf method, which allows us to solve the equations analytically [32–34]. Additional factors such as dissipation [11,20,31,34] and formation of alternating strips of compressible and incompressible phases near the edge [8,13–15,30,31,35–38] make the theory of edge magnetoplasmons more complicated. The basic feature of a local structure of electronic states near the edge in magnetic field is formation of magnetic edge channels [39] due to the upward bending of Landau levels caused either by hard boundary of the

sample (see Fig. 1) or by soft confinement field. In the latter picture with the soft edge taken at the classical level, the lateral electric field which confines electrons inside a sample drives electrons into a spiraling motion in crossed electric and magnetic fields with some average *drift velocity*. Switching to the reference frame moving with the drift velocity, where the electric field vanishes, we obtain simple addition of the
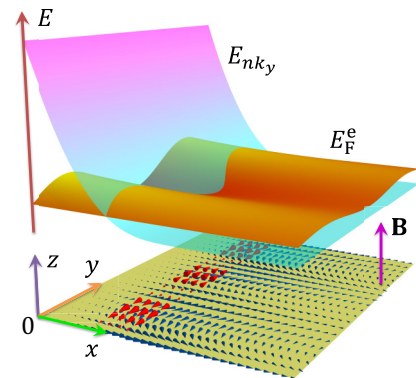

FIG. 1. Illustration of the origin of edge magnetoplasmon drift velocity. Wavelike oscillations of the local Fermi level E_F^e change the filling of magnetic edge channels, i.e., Landau levels with the energies E_{nk_y}, which are bent upward near the edge $x = 0$. Since the edge channels are unidirectional, oscillations of their occupation give rise to oscillations of edge current, shown by red cones. The edge current appears in phase with the bulk current response of the 2DEG (blue cones) and thus effectively enhances its Hall conductivity σ_{xy}. The edge magnetoplasmon velocity, which is roughly proportional to $|\sigma_{xy}|$, is increased too by the quantity v_{dr}, which has the meaning of drift velocity.

*asokolik@hse.ru

drift velocity to the magnetoplasmon velocity, which is predicted by the edge mode theory without taking into account the carrier drift. Such classical-level addition of velocities was used to interpret data of several experiments [21,22,28]. Alternative explanations of the extra edge magnetoplasmon velocity are based on local capacitance models [6,8,15], and recent analysis uses the model of chiral linearly-dispersive edge states [27].

In this paper, we develop the fully quantum theory of drift velocity of edge magnetoplasmons, which starts from the analysis of electron states near the hard edge of 2DEG in magnetic field (magnetic edge channels), presented in Sec. II. As shown schematically in Fig. 1, perturbations of a local Fermi level near the edge during magnetoplasma oscillations induce the linear responses of oscillating charge and current densities, which are also confined to the edge on a scale of magnetic length. The drift velocity v_{dr} arises in our theory as the joint characteristic of charge and density responses of the magnetic edge channels, and we derive the analytical expression for it as harmonic mean of group velocities of those edge states which cross the Fermi level. The additional current and density responses of the edge channels, which should be taken into account together with the bulk response of 2DEG, give rise to additional terms in equations describing the edge magnetoplasmons. Solving these equations analytically using the Wiener-Hopf method in Sec. III, we show that the edge response effectively enhances the bulk Hall conductivity of 2DEG and thus increases the total magnetoplasmon velocity. In Sec. IV, we present calculations of the edge magnetoplasmon dispersion and analyze its long-wavelength limit. We show that in this limit, v_{dr} is approximately added to the magnetoplasmon velocity obtained without taking into account the edge response. Moreover, in the limit of a large number of occupied Landau levels, v_{dr} tends to the average velocity of electron spiraling motion in the effective confining electric field superimposed on the magnetic field. These results agree with the conventional classical picture, but here we obtain them from the first principles. Section V is devoted to conclusions, and the Appendix provides details about quasiclassical calculations of the drift velocity.

II. EDGE CHANNELS AND THEIR RESPONSE

Consider the edge states of electrons on the boundary of 2DEG, which occupies the half-plane $x \geqslant 0$, $z = 0$. The uniform external magnetic field $\mathbf{B} = \mathbf{e}_z B$ corresponds to the vector potential $\mathbf{A} = \mathbf{e}_y Bx$ taken in the Landau gauge. Electron wave functions can be found as $\psi(x, y) = L_y^{-1/2} e^{ik_y y} \phi(x)$, where k_y is the electron momentum along the edge, L_y is the system size in the y direction, and $\phi(x)$ obeys the Schrodinger equation

$$-\frac{\hbar^2}{2m}\phi''(x) + \frac{1}{2m}\left(\hbar k_y + \frac{eBx}{c}\right)^2 \phi(x) = E\phi(x) \quad (1)$$

(hereafter we take the electron charge equal to $-e$, where $e > 0$). For a hard edge, we impose the Dirichlet boundary condition $\phi(0) = 0$. The general solution of Eq. (1), which is normalizable at the half-line $x \geqslant 0$, is given by the parabolic cylinder functions $U(-\varepsilon, z)$ [40]. The full electron wave func-
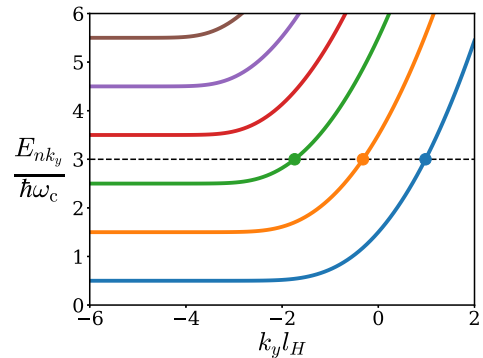

FIG. 2. Energies of the edge states E_{nk_y} in magnetic field as functions of the wave vector k_y along the edge. The curves from bottom to top correspond to the levels $n = 0 \ldots 5$. Dashed line shows the example of Fermi level location E_F^e between the bulk Landau levels $n = 2$ and 3, and circles demonstrate its intersections with the edge state energies at momenta k_n^{max}, $n = 0, 1, 2$.

tion reads

$$\psi_{nk_y}(x, y) = \frac{e^{ik_y y}}{\sqrt{L_y l_H} N_{nk_y}} U\left(-\varepsilon_{nk_y}, \frac{\sqrt{2}}{l_H}\left(x + l_H^2 k_y\right)\right), \quad (2)$$

and the corresponding energy of the nth stationary state $E_{nk_y} = \hbar\omega_c \varepsilon_{nk_y}$ is related to the dimensionless energy ε_{nk_y}, which can be found as the $(n + 1)$th (in the increasing order, $n = 0, 1, 2, \ldots$) root of the equation

$$U\left(-\varepsilon_{nk_y}, \sqrt{2}l_H k_y\right) = 0. \quad (3)$$

Here $\hbar\omega_c = \hbar eB/mc$ and $l_H = \sqrt{\hbar c/eB}$ are, respectively, cyclotron energy and magnetic length, which determine characteristic energy and length scales of electron quantum states in magnetic field. The factor N_{nk_y} is determined by the wave function normalization condition: $\int_0^\infty dx \int_0^{L_y} dy |\psi_{nk_y}(x, y)|^2 = 1$.

Edge-state energies at different n as functions of k_y are shown in Fig. 2. At $k_y \to -\infty$, the center of wave function accumulation $x \approx -l_H^2 k_y$ moves away from the edge $x = 0$ to the bulk $x \to \infty$. The influence of the boundary weakens, so the edge state wave functions and energies tend to those of ordinary Landau levels [41] in unbounded 2DEG in magnetic field,

$$\psi_{nk_y}^L(x, y) = \frac{e^{ik_y y} e^{-(x+l_H^2 k_y)^2/2l_H^2}}{\sqrt{2^n n! L_y l_H \sqrt{\pi}}} H_n\left(\frac{x + l_H^2 k_y}{l_H}\right), \quad (4)$$

$$E_n^L = \hbar\omega_c\left(n + \frac{1}{2}\right), \quad (5)$$

where H_n are Hermite polynomials. In the opposite limit $k_y \to \infty$, the wave functions are strongly squeezed against the edge potential wall, so the energies tend to the classical limit $E_{nk_y} \sim \hbar^2 k_y^2/2m$, which describes electron states freely propagating along the edge. The Appendix presents a
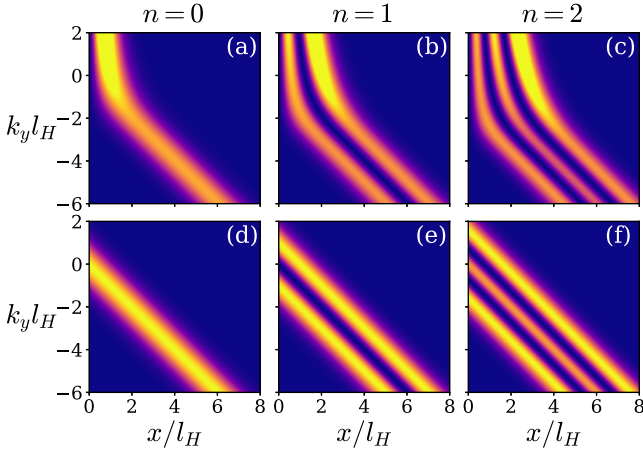
FIG. 3. Wave function square moduli $|\psi|^2$ for (a)–(c) edge states (2), (d)–(f) bulk Landau levels (4) at different wave vectors k_y along the edge. The columns correspond to the level numbers $n = 0, 1, 2$.
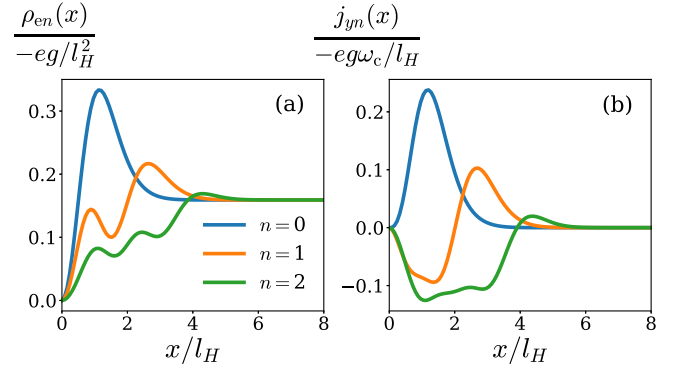

FIG. 4. Contributions (9) and (10) of individual edge channels $n = 0, 1, 2$ to (a) charge density $\rho_e(x)$ and (b) current density $j_y(x)$ as functions of the distance x from the edge. The Fermi level E_F^e is located in the midgap between the bulk Landau levels $n = 2$ and 3, as shown in Fig. 2.

more accurate formula (A6) for edge-state energies applicable at $l_H k_y > -\sqrt{2n+1}$, which is derived using quasiclassical quantization. Figures 3(a)–3(c) show square moduli of the edge-state wave functions (2) for $n = 0, 1, 2$, and Figs. 3(d)–3(f) show square moduli of bulk Landau level (or displaced harmonic oscillator) wave functions (4) which could exist without the Dirichlet boundary condition at $x = 0$. The wave functions in the top and bottom rows become progressively similar at $k_y \to -\infty$.

Occupation of the edge states (2) by electrons gives rise to the following spatial profiles of charge density and current density along the edge:

$$\rho_e(x) = -eg \sum_{nk_y} f_{nk_y} |\psi_{nk_y}(x, y)|^2, \tag{6}$$

$$j_y(x) = -\frac{eg}{m} \sum_{nk_y} f_{nk_y} \left(\hbar k_y + \frac{eBx}{c} \right) |\psi_{nk_y}(x, y)|^2. \tag{7}$$

Here $g = 2$ is the spin degeneracy factor for electron states, f_{nk_y} are occupation numbers of edge states which, at low temperatures, follow the steplike energy dependence $f_{nk_y} = \Theta(E_F^e - E_{nk_y})$, where E_F^e is the local Fermi level near the edge and $\Theta(x)$ is the unit step function. We need to sum over momenta k_y of the occupied edge states in Eqs. (6) and (7), which are integer multiples of $2\pi/L_y$ in a sample with periodic boundary conditions along the y axis. As seen from Fig. 2, this summation should be carried out from $-\infty$ to the maximal values $k_n^{\max}$, which are different for each n. These values are given by the condition $E_{nk_n^{\max}} = E_F^e$ or, using Eq. (3), by the equation

$$U\left(-E_F^e/\hbar\omega_c, \sqrt{2}l_H k_n^{\max} \right) = 0. \tag{8}$$

Separating in Eqs. (6) and (7) contributions of different levels n as $\rho_e(x) = \sum_n \rho_{en}(x)$, $j_y(x) = \sum_n j_{yn}(x)$, and switching from summation over k_y to integration in the limit $L_y \to \infty$,

we obtain

$$\rho_{en}(x) = -\frac{eg}{2\pi l_H} \int_{-\infty}^{k_n^{\max}} dk_y \frac{U^2(-\varepsilon_{nk_y}, \sqrt{2}(k_y l_H + x/l_H))}{|N_{nk_y}|^2}, \tag{9}$$

$$j_{yn}(x) = -\frac{eg\omega_c}{2\pi} \int_{-\infty}^{k_n^{\max}} dk_y (k_y l_H + x/l_H)$$
$$\times \frac{U^2(-\varepsilon_{nk_y}, \sqrt{2}(k_y l_H + x/l_H))}{|N_{nk_y}|^2}. \tag{10}$$

Note that $\rho_{en}(x) = 0$, $j_{yn}(x) = 0$ when $E_n^L \leqslant E_F^e$, because in this case the whole nth edge state is unoccupied.

Figure 4 shows the example of how the nth edge channels contribute to spatial profiles of the charge and current densities. These profiles are confined to the distance $x \sim l_H$ of several magnetic lengths from the edge $x = 0$. Note that each charge density profile $\rho_{en}(x)$ tends at $x \to \infty$ to the universal value $-eg/2\pi l_H^2$ equal to the charge density of a single completely filled bulk Landau level. Since we are interested only in variations of charge density during magnetoplasma oscillations due to transient changes of edge-state occupations, we subtract this constant part by considering not the charge density itself $\rho_e(x)$, but its local deviation from the bulk value near the edge: $\tilde{\rho}_{en}(x) = \rho_{en}(x) + eg/2\pi l_H^2$, $\tilde{\rho}_e(x) = \rho_e(x) + n_0 eg/2\pi l_H^2$, where n_0 is the number of completely filled bulk Landau levels, which depends on the bulk Fermi level location.

Taking into account that local variations of charge and current densities near the edge are confined to a region of several magnetic lengths, which is small in strong magnetic field in the quantum Hall regime, we can look only on the integral charge (per unit length of the edge) $Q_e = \sum_n Q_{en}$, $Q_{en} = \int_0^\infty dx \, \tilde{\rho}_{en}(x)$, and integral current along the edge $I_y = \sum_n I_{yn}$, $I_{yn} = \int_0^\infty dx \, j_{yn}(x)$ both resolved over edge channels numbers n. These quantities can be found analytically. First, representing the bulk charge density $-eg/2\pi l_H^2$ as the k_y-integrated density $-eg|\psi_{nk_y}^L|^2$ provided by the bulk Landau

levels (4), we obtain from Eq. (9):

$$Q_{en} = -\frac{egL_y}{2\pi} \int_0^\infty dx \left\{ \int_{-\infty}^{k_n^{max}} dk_y \, |\psi_{nk_y}(x,y)|^2 \right.$$

$$\left. - \int_{-\infty}^\infty dk_y \, |\psi_{nk_y}^L(x,y)|^2 \right\} = -\frac{eg}{2\pi} k_n^{max}. \quad (11)$$

The last equality was obtained by changing the order of integration over x and k_y [which is possible due to rapid decay of the integrand $|\psi_{nk_y}(x,y)|^2 - |\psi_{nk_y}^L(x,y)|^2$ at $x \to \infty$, $k_y \to -\infty$, see Fig. 3] and using the symmetry property $|\psi_{nk_y}^L(x,y)|^2 = |\psi_{n,-k_y}^L(-x,y)|^2$. Second, using the Hellmann-Feynman theorem $\partial E_{nk_y}/\partial k_y = \langle \psi_{nk_y} | \partial H/\partial k_y | \psi_{nk_y} \rangle$, we can easily integrate Eq. (10) by x, so the integral edge current reads

$$I_{yn} = -\frac{eg}{2\pi\hbar} \int_{-\infty}^{k_n^{max}} dk_y \frac{\partial E_{nk_y}}{\partial k_y} = -\frac{eg}{2\pi\hbar} \left(E_F^e - E_n^L\right). \quad (12)$$

Summing contributions of all partially occupied edge channels with $E_F^e > E_n^L$, we obtain the following simple expressions for integral charge and current at the edge:

$$Q_e = -\frac{eg}{2\pi} \sum_n \Theta\left(E_F^e - E_n^L\right) k_n^{max}, \quad (13)$$

$$I_y = -\frac{eg}{2\pi\hbar} \sum_n \Theta\left(E_F^e - E_n^L\right)\left(E_F^e - E_n^L\right). \quad (14)$$

III. THEORY OF MAGNETOPLASMONS WITH EDGE CHARGE AND CURRENT

Now we consider the problem of edge magnetoplasmons propagating along the straight boundary of 2D conducting material. Suppose the electric potential φ and the oscillating charge density ρ on the surface of the 2D material have the common plane-wave dependence on y and t: $\varphi, \rho \propto e^{i(qy-\omega t)}$ (we assume $q, \omega > 0$). At each point (x, y) of this material, the 2D current density $\mathbf{j} = \{j_x, j_y\}$ can be found as the matrix product of the local conductivity tensor $\sigma_{\alpha\beta}(x)$ and the electric field vector $\mathbf{E} = -\nabla\varphi = \{-\varphi'(x), -iq\varphi(x)\}$:

$$j_x = -\sigma_{xx}(x)\varphi'(x) - iq\sigma_{xy}(x)\varphi(x), \quad (15)$$

$$j_y = -\sigma_{yx}(x)\varphi'(x) - iq\sigma_{yy}(x)\varphi(x) + \Delta j_y^{dr}(x). \quad (16)$$

The key point here is the density of *drift current* Δj_y^{dr} in the right-hand side of Eq. (16), which is the oscillating part $\Delta j_y^{dr} \propto e^{i(qy-\omega t)}$ of the boundary current (14) carried by the edge channels and distributed in space near the sample boundary as shown in Fig. 4(b). This term is absent in the conventional theory of edge modes [1,29–34,42]. The oscillations of drift current density Δj_y^{dr} originate from transient changes of the edge state occupations due to oscillations $\Delta E_F^e \propto e^{i(qy-\omega t)}$ of the local Fermi level at the edge $E_F^e = E_F + \Delta E_F^e$ around its equilibrium bulk value E_F, see Fig. 1. If the amplitude of these oscillations is relatively small, we assume the linear response of magnetic edge channels taking small oscillating perturbations of Eqs. (13) and (14): $\Delta Q_e = (\partial Q_e/\partial E_F^e)\Delta E_F^e$, $\Delta I_y = (\partial I_y/\partial E_F^e)\Delta E_F^e$.

The oscillating integral edge current $\Delta I_y = \int_0^\infty dx \, \Delta j_y^{dr}(x)$ is distributed over several magnetic lengths near the edge $x =$

0, as seen from Fig. 4(b). We can introduce the model distribution function $a(x)$, which is essentially nonzero near $x = 0$ on the scale $x \sim l_H$ and normalized to unity, such as $\Delta j_y^{dr}(x) = a(x)\Delta I_y$, $\int_{-\infty}^\infty dx \, a(x) = 1$. The coordinate-dependent components $\sigma_{\alpha\beta}(x)$ of the conductivity tensor rise from zero in empty space $x < 0$ to their bulk values $\sigma_{\alpha\beta}$ at $x \to \infty$. This also happens on the scale of several magnetic lengths, so, for simplicity of the following calculations, we can assume that $\partial_x \sigma_{\alpha\beta}(x) = a(x)\sigma_{\alpha\beta}$. As will be clear below, the exact shape of the function $a(x)$ is not important as long as the charge density $\rho(x)$ and electric potential $\varphi(x)$ profiles of magnetoplasmon oscillations are slowly varying on the scale of l_H. Thus, using the continuity equation $\partial\rho/\partial t + \text{div } \mathbf{j} = 0$, which in our case turns into $-i\omega\rho + \partial_x j_x + iq j_y = 0$, we obtain from Eqs. (15) and (16):

$$i\omega\rho(x) = a(x)\{-\sigma_{xx}\varphi'(x) - iq\sigma_{xy}\varphi(x) + iq\Delta I_y\}$$
$$- iq(\sigma_{xy} + \sigma_{yx})\varphi'(x) - \sigma_{xx}\varphi''(x) + \sigma_{yy}q^2\varphi(x). \quad (17)$$

For isotropic material in magnetic field, $\sigma_{xx} = \sigma_{yy}$, $\sigma_{xy} = -\sigma_{yx}$, so the second term on the right-hand side vanishes.

The oscillations ΔE_F^e of the local Fermi level at the edge can be related to those of the integral charge ΔQ_e, so $\Delta I_y = (\partial I_y/\partial E_F^e)(\partial Q_e/\partial E_F^e)^{-1}\Delta Q_e$. In strong enough magnetic field, where l_H is much smaller than the characteristic length scale of $\varphi(x)$, which is known to be of the order of q^{-1} [32,42], we can replace $a(x)$ by the Dirac delta function, $a(x) \approx \delta(x)$. Thus, Eq. (17) takes the form

$$i\omega\rho(x) = \delta(x)\left\{-\sigma_{xx}\varphi'(x) - iq\left[\sigma_{xy} - v_{dr}\frac{\Delta Q_e}{\varphi(0)}\right]\varphi(0)\right\}$$
$$- \sigma_{xx}\left(\partial_x^2 - q^2\right)\varphi(x), \quad (18)$$

where the drift velocity

$$v_{dr} = \frac{\partial I_y}{\partial Q_e} = \left.\frac{\partial I_y/\partial E_F^e}{\partial Q_e/\partial E_F^e}\right|_{E_F^e = E_F} \quad (19)$$

was introduced. This velocity jointly characterizes the charge and density responses of the edge channels and can be calculated explicitly from Eqs. (13) and (14). Assuming that the Fermi level lies between n_0th and $(n_0 + 1)$th bulk Landau levels, $n_0 + \frac{1}{2} < E_F/\hbar\omega_c < n_0 + \frac{3}{2}$, so $n_0 + 1$ edge channels contribute to the sums in Eqs. (13) and (14), we obtain

$$v_{dr} = \frac{(n_0 + 1)/\hbar}{\sum_{n=0}^{n_0} \frac{\partial k_n^{max}}{\partial E_{nk_y}}} = \left\langle \left(\frac{1}{\hbar}\frac{\partial E_{nk_y}}{\partial k_y}\right)^{-1} \right\rangle^{-1}, \quad (20)$$

where the average $\langle \dots \rangle$ is taken at the Fermi level $E_{nk_y} = E_F$ over all edge states crossing this level. Thus, we may interpret v_{dr} as a *harmonic mean of group velocities* of all magnetic edge channels crossing the Fermi level.

Equation (18) has a form of conventional continuity equation in the theory of plasmon-type edge modes [29–32,34,42], but with the Hall conductivity σ_{xy} replaced by

$$\tilde{\sigma}_{xy} = \sigma_{xy} - v_{dr}\frac{\Delta Q_e}{\varphi(0)} \quad (21)$$

due to the response of edge channels. Since in magnetic field along the positive z axis with negatively charged carriers

$\sigma_{xy} < 0$ at low frequencies $\omega \to 0$, and $\Delta Q_e / \varphi(0) > 0$, the edge channels effectively increase the negative σ_{xy} by the absolute value. In other words, the current response of edge channels acts in phase with the bulk currents caused by the Hall conductivity, as depicted in Fig. 1. As will be shown below [see Eq. (43)], in the long-wavelength limit the magnetoplasmon phase velocity ω/q is approximately proportional to $|\sigma_{xy}|$ [32–34], thus the edge channel response speeds up the magnetoplasmons.

We need to supplement Eq. (18) with the Poisson equation $\varepsilon_b \nabla^2 \varphi = -4\pi \rho \delta(z)$, where ε_b is the background dielectric constant of the surrounding medium. For a half-plane material, this equation at $z = 0$ can be transformed into the integral form [1,32–34]

$$\varphi(x) = \frac{4\pi}{\varepsilon_b} \int_0^\infty dx' \, L(x - x') \rho(x'), \qquad (22)$$

where the kernel

$$L(x - x') = \int_{-\infty}^\infty \frac{dk}{2\pi} \frac{e^{ik(x-x')}}{2\sqrt{k^2 + q^2}} = \frac{1}{2\pi} K_0(q|x - x'|) \quad (23)$$

is given in terms of the second kind Bessel function K_0.

The system of equations (18), (22) can be solved analytically using the Wiener-Hopf method [32–34,42–44] after the Fourier transforms of $\varphi(x)$ and $\rho(x)$ are carried out separately at $x < 0$ and $x > 0$: $\Phi_+(\xi) = \int_0^\infty dx \, e^{iq\xi x} \varphi(x)$, $\Phi_-(\xi) = \int_{-\infty}^0 dx \, e^{iq\xi x} \varphi(x)$, $Q_+(\xi) = \int_0^\infty dx \, e^{iq\xi x} \rho(x)$. Applying these transforms to Eqs. (18) and (22), we obtain

$$i\omega Q_+(\xi) = -iq\varphi(0)(\xi \sigma_{xx} + \tilde{\sigma}_{xy}) + q^2 \sigma_{xx}(\xi^2 + 1)\Phi_+(\xi), \qquad (24)$$

$$\Phi_+(\xi) + \Phi_-(\xi) = \frac{4\pi}{\varepsilon_b q} L(\xi) Q_+(\xi), \qquad (25)$$

where, according to Eq. (23), the dimensionless Fourier-transformed kernel is $L(\xi) = [2\sqrt{\xi^2 + 1}]^{-1}$. Excluding Q_+ from Eqs. (24) and (25), we obtain

$$\varepsilon(\xi)\Phi_+(\xi) + \Phi_-(\xi) = -\frac{i\varphi(0)}{q} L(\xi)(\eta\xi - i\tilde{\chi}), \qquad (26)$$

where the dielectric function of the 2D material,

$$\varepsilon(\xi) = 1 - \eta L(\xi)(\xi^2 + 1) = 1 - \frac{\eta}{2}\sqrt{\xi^2 + 1}, \qquad (27)$$

at the wave vector $\mathbf{k} = \{-q\xi, q\}$ is introduced. The dimensionless conductivities

$$\eta = \frac{4\pi q \sigma_{xx}}{i\varepsilon_b \omega}, \quad \chi = \frac{4\pi q \sigma_{xy}}{\varepsilon_b \omega} \qquad (28)$$

are purely real in the static nondissipative limit, when σ_{xx} and σ_{xy} are, respectively, imaginary and real. Since σ_{xy} is renormalized, see Eq. (21), due to the edge channel response, χ gets renormalized as well:

$$\tilde{\chi} = \chi - \frac{4\pi q v_{dr}}{\varepsilon_b \omega} \frac{\Delta Q_e}{\varphi(0)}. \qquad (29)$$

According to the definitions, the functions $\Phi_+(\xi)$ and $\Phi_-(\xi)$ are analytical in, respectively, the upper and lower half-planes of the complex dimensionless wave vector ξ. The Wiener-Hopf method [32,44] relies on the decomposition $\varepsilon(\xi) = F_+(\xi)/F_-(\xi)$ of the dielectric function (27), where

$F_\pm(\xi)$ are analytical in, respectively, upper and lower half-planes. This decomposition can be carried out analytically (see also Ref. [45]), and the result is

$$F_+(\xi) = -\frac{\eta}{2} \frac{(1 - z_1)^{(s+1)/2}(1 + z_2)^{1/2}}{(2p)^{1/2}(1 + z_1)^{s/2}} K(\xi), \qquad (30)$$

$$F_-(\xi) = \frac{(2p)^{1/2}(1 + z_2)^{s/2}}{(1 + z_1)^{1/2}(1 - z_2)^{(s+1)/2}} K(\xi), \qquad (31)$$

$$K(\xi) = \exp\left\{\frac{\pi i}{4} + \frac{s}{2\pi i}[f(z_1) + f(z_2)]\right\}, \qquad (32)$$

$$f(z) = -\frac{\pi^2}{6} + \log z \log(1 + z) + \text{Li}_2(-z) + \text{Li}_2(1 - z), \qquad (33)$$

where $z_1 = isp\lambda$, $z_2 = -isp/\lambda$, $s = \text{sign}(\text{Re}\,\eta)$, $p = \xi + \sqrt{\xi^2 + 1}$, $\lambda = -2i/\eta + \sqrt{1 - (2/\eta)^2}$; Li_2 is the dilogarithm function. These formulas are applicable for any complex η, i.e., in both capacitive ($\text{Im}\,\sigma_{xx} < 0$, $\text{Re}\,\eta < 0$) and inductive ($\text{Im}\,\sigma_{xx} > 0$, $\text{Re}\,\eta > 0$) regimes of the conductivity, and for both materials with dissipation ($\text{Re}\,\sigma_{xx} > 0$, $\text{Im}\,\eta < 0$) and active media ($\text{Re}\,\sigma_{xx} < 0$, $\text{Im}\,\eta > 0$).

Equating separately the parts of Eq. (26), which are analytical in upper and lower complex half-planes of ξ, we obtain the Fourier transforms of the potential (see the details in Refs. [32,42]):

$$\Phi_\pm(\xi) = \pm \frac{i\varphi(0)}{2q}\left\{\frac{1 - \tilde{\chi}/\eta}{\xi - i}\left[1 - \frac{F_+(i)}{F_\pm(\xi)}\right] + \frac{1 + \tilde{\chi}/\eta}{\xi + i}\left[1 - \frac{F_-(-i)}{F_\pm(\xi)}\right]\right\}. \qquad (34)$$

At $|\xi| \to \infty$, the functions (30) and (31) behave as $F_\pm(\xi) \propto \xi^{\pm 1/2}$, which allows us to find the power-law asymptotics of $\Phi_\pm(\xi)$ at large ξ. They are related to the limiting behavior of the potential $\varphi(x) = q \int_{-\infty}^\infty d\xi \, e^{-iq\xi x}[\Phi_+(x) + \Phi_-(x)]$ at $x \to 0$. By equating the limiting value $\varphi(x \to 0)$ to $\varphi(0)$ in Eq. (34), we find the dispersion equation for edge magnetoplasmons:

$$(\eta - \tilde{\chi})F_+(i) + (\eta + \tilde{\chi})F_-(-i) = 0. \qquad (35)$$

Using the analytical expressions (30) and (31), this equation can be written explicitly as

$$\frac{F_+(i)}{F_-(-i)} = \frac{1 + \lambda}{1 - \lambda} \exp\left\{\frac{2i}{\pi} f(\lambda)\right\} = \frac{\tilde{\chi} + \eta}{\tilde{\chi} - \eta}. \qquad (36)$$

To calculate the magnetoplasmon dispersion from Eq. (36), taking into account the edge channel response (29), we need to find the ratio $\Delta Q_e / \varphi(0)$, which defines the fraction of a total magnetoplasmon oscillating charge which is accommodated by the edge channels. The theory of edge modes [32,42] shows that oscillating charge density $\rho(x)$ behaves as $\rho(x) \propto x^{-1/2}$ at the distances from the edge $x = 0$ much smaller than the wavelength $2\pi/q$. Thus, we can assume that the dominating part of the charge is concentrated in a very narrow strip near the edge, so $\Delta Q_e \approx \int_0^\infty dx \, \rho(x) = Q_+(0)$. From Eqs. (25), (34), and (35) we can find the Fourier transform of charge density:

$$Q_+(\xi) = \frac{\varphi(0)\varepsilon_b}{4\pi}(\eta - \tilde{\chi})\frac{F_+(i)}{F_+(\xi)}. \qquad (37)$$

Using the property $F_+(\xi)F_-(-\xi) = -\eta/2$ of the functions $F_\pm(\xi)$ and the dispersion equation (35), we obtain $F_+(0) = -(\eta/2)\sqrt{1-2/\eta}$ and $F_+(i) = \sqrt{\eta(\eta+\tilde\chi)/2(\eta-\tilde\chi)}$ (we take into account here that $\eta, \tilde\chi < 0$ for a system in the quantum Hall regime at low frequencies of edge magnetoplasmons). Thus, Eq. (37) at $\xi = 0$ results in

$$\Delta Q_e = Q_+(0) = \frac{\varphi(0)\varepsilon_b}{4\pi}\frac{\sqrt{\tilde\chi^2-\eta^2}}{\sqrt{1-\eta/2}}. \quad (38)$$

Substituting Eq. (38) to Eq. (29), we obtain

$$\tilde\chi = \chi - \frac{qv_{dr}}{\omega}\frac{\sqrt{\tilde\chi^2-\eta^2}}{\sqrt{1-\eta/2}}. \quad (39)$$

Equations (36) and (39), taken with the notations (19) and (28), and with the edge channel charge and current response functions (13) and (14), are the main result of this paper. These equations determine the edge magnetoplasmon dispersion $\omega(q)$ when the edge channel response, characterized by the drift velocity v_{dr}, is taken into account.

IV. EDGE MAGNETOPLASMON DISPERSIONS

From the point of view of the existing experiments on edge magnetoplasmons [8–11,20,21], only the long-wavelength asymptotic of the dispersion relation $\omega(q)$ at $q, \omega \to 0$ is usually relevant and observable. In this limit, for a conducting material with negligible dissipation, which turns into an insulator in the quantum Hall regime, the parameter $\eta = 4\pi q\sigma_{xx}/i\varepsilon_b\omega$ is small by the absolute value and negative. We can represent it as $\eta = -2qw$, where $w = -(2\pi/\varepsilon_b)(\partial\mathrm{Im}\sigma_{xx}/\partial\omega)|_{\omega=0}$ is the characteristic penetration length of the charge density oscillations (the 2D counterpart of a 3D conductor skin depth) [32,34]. The parameter $\chi = 4\pi q\sigma_{xy}/\varepsilon_b\omega$ remains finite and negative at $q, \omega \to 0$. The asymptotic expressions for the functions (30) and (31) at $\eta \to 0$ can be written as

$$F_\pm(\xi) = \sqrt{-\frac{\eta}{2}}\left\{1 - \frac{i\eta}{4\pi p}\left[(p^2+1)\left(\mp\frac{\pi i}{2}+\log p\right)\right.\right.$$
$$\left.\left.+(p^2-1)\log\left(-\frac{\eta}{4\mathfrak{e}}\right)\right]+O(\eta^2)\right\}, \quad (40)$$

where $\mathfrak{e}$ is the base of a natural logarithm. Using these asymptotics, we obtain

$$\frac{F_+(i)}{F_-(-i)} \approx 1 + \frac{\eta}{\pi}\log\left(-\frac{\eta}{4\mathfrak{e}}\right), \quad (41)$$

so we bring the dispersion equation (36) to the approximate form

$$\frac{1}{\tilde\chi-\eta} = \frac{1}{2\pi}\log\left(-\frac{\eta}{4\mathfrak{e}}\right). \quad (42)$$

Taking into account that $|\eta| \ll |\tilde\chi|$ at $\omega \to 0$ and using Eqs. (28) and (39), we obtain the magnetoplasmon dispersion in the long-wavelength limit:

$$\omega \approx v_{dr}q - \frac{2\sigma_{xy}q}{\varepsilon_b}\log\frac{2\mathfrak{e}}{qw}. \quad (43)$$

This formula differs by the drift term $v_{dr}q$ from the well-known asymptotic formula for edge magnetoplasmon
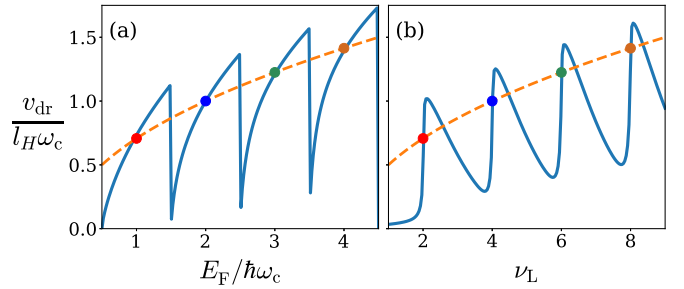

FIG. 5. Drift velocity v_{dr} (solid lines) as function of (a) Fermi level E_F and (b) Landau-level filling factor ν_L. Dashed lines show the quasiclassical approximation (44) which coincides (circles) with the exact quantum-mechanical v_{dr} when the Fermi level is located in the midgap between Landau levels, i.e., when $E_F/\hbar\omega_c$ and $\frac{1}{2}\nu_L$ are equal integers.

dispersion [32,34]. Thus, due to the additional current response of the magnetic edge channels, the edge magnetoplasmon phase velocity $v = \omega/q$ increases by v_{dr}.

Although our analysis started from the hard-edge boundary conditions, this result is surprisingly consistent with the classical picture of the soft edge formed by a local electric field $\mathcal{E}_x^{conf}$ which confines electrons inside the sample. Indeed, such field gives rise to a spiraling motion of the electrons in magnetic field with the *classical* drift velocity $v_{dr}^c = -c\mathcal{E}_x^{conf}/B$ along the edge. On the other hand, the edge state wave function is typically concentrated near $x_0 = -l_H^2 k_y$ (at least, when $k_y \to -\infty$, see Fig. 3), so we can relate the x_0 and k_y derivatives of edge-state energies to obtain the effective confining field in terms of mean force $F_x = -e\mathcal{E}_x^{conf} = -\partial E_{nk_y}/\partial x_0 \approx l_H^{-2}\partial E_{nk_y}/\partial k_y$ acting on electrons at the Fermi level near the edge. Hence the classical drift velocity is $v_{dr}^c = \hbar^{-1}(\partial E_{nk_y}/\partial k_y)$, which agrees with the quantum-mechanical expression (20) if we neglect the variance of edge-state group velocities.

The *quasiclassical* approximation for v_{dr} can be obtained from Eq. (20) in the limit when a large number of bulk Landau levels $n_0 = E_F/\hbar\omega_c - 1 \gg 1$ are occupied, and when we find the edge-state energies E_{nk_y} approximately using the quasiclassical quantization condition. As shown in the Appendix:

$$v_{dr}^{qc} = l_H\omega_c\sqrt{\frac{n_0+1}{2}} = \sqrt{\frac{E_F}{2m}}. \quad (44)$$

Assuming that the Fermi energy $E_F = \frac{1}{2}mv_F^2$ can be related to the Fermi velocity v_F of electrons at the edge, we obtain $v_{dr}^{qc} = \frac{1}{2}v_F$. This estimate agrees with Ref. [46], where the velocity of quasiclassical motion on skipping orbits in magnetic field was found to be of the order of the Fermi velocity, and with the recent experiment [28].

The drift velocity v_{dr}, calculated according to quantum-mechanical formulas (19), (13), and (14), is shown in Fig. 5 as function of the Fermi level E_F and Landau-level filling factor ν_L, i.e., number of occupied Landau levels, taking into account their double spin degeneracy g. To calculate the ν_L dependence, a weak broadening of the Landau levels is assumed, which makes the dependence of E_F on the electron density $n_e = \nu_L/2\pi l_H^2$ almost steplike, but smooth, when the system

goes through a sequence of interchanging compressible and incompressible phases [8,35]. As seen in Fig. 5, the quasi-classical approximations (44) coincide with the exact result (19) when the Landau-level filling is strictly integer, i.e., in the incompressible phases when the Fermi level is located in the midgaps. In the following, we will consider only such cases of integer Landau level fillings corresponding to the quantum Hall regime, when $E_F/\hbar\omega_c = n_0 + 1 = \nu_L/g$.

To calculate the conductivity tensor $\sigma_{\alpha\beta}(\omega)$ of 2DEG in magnetic field, we can use the approach similar to those applied to graphene in Ref. [34]. In the $\mathbf{E} \cdot \mathbf{r}$ gauge, with the assumption of Lorentzian broadening of the spectral function $A_n(E) = (\Gamma/\pi)/[(E - E_n^L)^2 + \Gamma^2]$ of each nth Landau level with the width Γ, we obtain

$$\sigma_{xx}(\omega) = \frac{ige^2\hbar\omega_c^2}{4\pi} \sum_{n=1}^{\infty} n[I_{n,n-1}(\omega) + I_{n-1,n}(\omega)], \quad (45)$$

$$\sigma_{xy}(\omega) = \frac{ge^2\hbar\omega_c^2}{4\pi} \sum_{n=1}^{\infty} n[I_{n,n-1}(\omega) - I_{n-1,n}(\omega)], \quad (46)$$

where

$$I_{n_1 n_2}(\omega) = \int dE_1 dE_2 \, A_{n_1}(E_1) A_{n_2}(E_2)$$
$$\times \frac{f(E_2) - f(E_1)}{(E_1 - E_2)(\hbar\omega + E_2 - E_1 + i\delta)}, \quad (47)$$

and $f(E) = \Theta(E_F - E)$ is the low-temperature occupation number of electronic state with the energy E. The integrals (47) take into account both inter-Landau-level electron transitions and intralevel transitions inside each broadened Landau level, in the case of its partial filling. In the case of integer Landau-level filling $E_F = \hbar\omega_c(n_0 + 1)$, and when the energy width of each level is much smaller than the cyclotron energy, $\Gamma \ll \hbar\omega_c$ (clean limit), we obtain $I_{n,n-1}(\omega) = \delta_{n,n_0+1}/\hbar^2\omega_c(\omega - \omega_c)$, $I_{n-1,n}(\omega) = \delta_{n,n_0+1}/\hbar^2\omega_c(\omega + \omega_c)$. The resulting conductivities of 2DEG in magnetic field calculated in the clean limit in the insulating (or incompressible) regime coincide with the classical Drude result:

$$\sigma_{xx}(\omega) = \frac{i\nu_L e^2}{2\pi\hbar} \frac{\omega\omega_c}{\omega^2 - \omega_c^2}, \quad \sigma_{xy}(\omega) = \frac{\nu_L e^2}{2\pi\hbar} \frac{\omega_c^2}{\omega^2 - \omega_c^2}. \quad (48)$$

The low-frequency asymptotics of these expressions $\sigma_{xx} \approx -(\varepsilon_b/2\pi)i\omega w$, $w = \nu_L e^2/\varepsilon_b\hbar\omega_c$, $\sigma_{xy} \approx -\nu_L e^2/2\pi\hbar$ can be used in Eq. (43) to find an approximate magnetoplasmon dispersion in the long-wavelength limit.

Calculation results for the edge magnetoplasmon dispersion in our approach depend on the dimensionless parameter

$$r_s = \frac{e^2/\varepsilon_b l_H}{\hbar\omega_c}, \quad (49)$$

which defines the ratio of characteristic Coulomb interaction and kinetic energies of electrons in magnetic field. As follows from Eqs. (43) and (44), the ratio of v_{dr} to the typical magnetoplasmon velocity $v = \omega/q \sim -\sigma_{xy}/\varepsilon_b$ found in the absence of the drift contribution behaves as $v_{dr}/v \sim 1/r_s$. Since $r_s \propto 1/\varepsilon_b\sqrt{B}$, we expect a significant contribution of v_{dr} to the total velocity of edge magnetoplasmon at strong
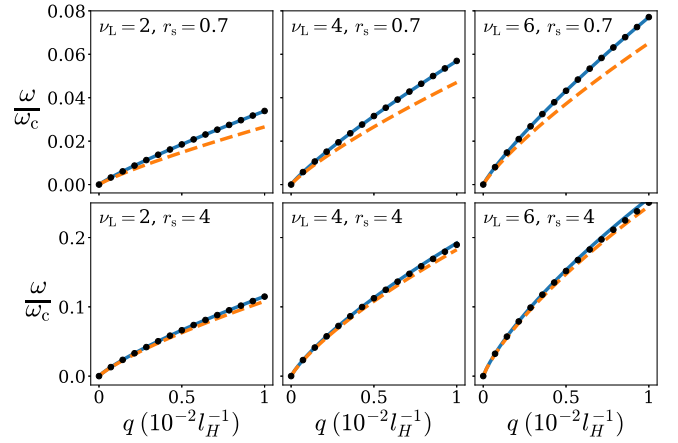

FIG. 6. Edge magnetoplasmon dispersions found numerically in the presence (solid lines) and absence (dashed lines) of the drift velocity v_{dr}. Black circles show the analytical approximation (43) for the long-wavelength limit. The panels correspond to different Landau level filling factors ν_L and Coulomb interaction strengths r_s.

dielectric screening or in strong magnetic field. In experiments on edge magnetoplasmons dealing with GaAs-based quantum wells [8–11], the system parameters are typically $\varepsilon_b = 4 - 13$, $B = 4 - 20$ T, and the electron effective mass is $m = 0.067m_0$, so $r_s \approx 0.6 - 4$. In the case of graphene [20,21], the role of cyclotron energy $\hbar\omega_c$ is played by the characteristic distance between Landau level $\hbar v_F/l_H$, where $v_F \approx 10^6$ m/s, so r_s does not depend on B but, depending on the substrate dielectric constant ε_b, can take the values $r_s \sim 2$ (for suspended graphene) or less.

Figure 6 shows the example results (solid lines) of the numerical solution of the dispersion equation (36), taking into account the contribution of the drift velocity. In experiments [6–25], typical wave numbers q of edge magnetoplasmons are $10 - 10^4$ cm^{-1}, while magnetic length is $l_H \sim 10$ nm at $B = 4 - 20$ T, so the dimensionless product ql_H does not exceed 10^{-2}. As seen in Fig. 6, in this regime the long-wavelength asymptotic (43), shown by black circles, proves to be quite accurate. For the sake of comparison, the dispersions calculated in the absence of v_{dr} are shown by dashed lines. The relative role of v_{dr} increases with decrease of r_s, in agreement with the arguments presented above. The total velocity of magnetoplasmons rises with increase of the filling factor ν_L, which agrees with experimental data [9,11,13,17].

We have considered the clean system, however, our analysis of the role of drift velocity remains valid in the presence of dissipation as well. Nonzero DC limit of conductivity $\lim_{\omega\to 0}\sigma_{xx}(\omega) = \sigma_{DC}$ implies that η acquires finite value $\eta = -4\pi iq\sigma_{DC}/\varepsilon_b\omega$ instead of being infinitesimally small. Since η is still much smaller by absolute value than $\tilde{\chi}$ in the strong magnetic field limit, it enters only the logarithm in the dispersion equation (42), so the approximation $\omega \approx -2\sigma_{xy}q/\varepsilon_b$ [see Eq. (43)] would be sufficient to estimate $\eta \approx 2\pi i\sigma_{DC}/\sigma_{xy}$. The resulting real part of the long-wavelength dispersion

$$\omega \approx v_{dr}q - \frac{2\sigma_{xy}q}{\varepsilon_b}\log\frac{2\mathfrak{e}|\sigma_{xy}|}{\pi\sigma_{DC}} \quad (50)$$

has the same form as in the clean limit (43) if the characteristic screening length is assumed to be $w = 2\pi\sigma_{\mathrm{DC}}/\varepsilon_{\mathrm{b}}\omega \approx \pi\sigma_{\mathrm{DC}}/q|\sigma_{xy}|$. The same expression for w in the presence of significant dissipation was derived in Ref. [32]. Thus, the additive contribution of v_{dr} to the total edge magnetoplasmon velocity arises in the long-wavelength limit irrespective of the role of dissipation.

V. CONCLUSIONS

Starting from quantum-mechanical analysis of magnetic edge channels, we developed consistent theory describing the drift velocity of edge magnetoplasmons. The unidirectional propagation of electrons populating the edge channels causes additional current response emerging during magnetoplasmon oscillations and accompanying perturbations of the local Fermi level near the edge. This response gives rise to additional term in the equations which describe edge magnetoplasmon electrodynamics. The magnitude of this term is characterized by the drift velocity v_{dr} calculated analytically as harmonic mean of group velocities of all magnetic edge channels whose dispersions cross the Fermi level. At the quasiclassical level, v_{dr} is analogous to the average velocity of electron spiraling motion in a confining electric field near the edge and in perpendicular magnetic field. As we show in the Appendix using the quasiclassical quantization, v_{dr} is close to one half of the electron Fermi velocity when a large number of Landau levels is occupied.

Due to Landau quantization, the quantum-mechanically calculated v_{dr} strongly oscillates when the Landau-level filling factor is changed, but on average it is close to one-half of the electron Fermi velocity, in agreement with the classical picture of skipping orbits. Assuming that charge density oscillations are confined in a narrow strip near the edge, we analytically solved the problem of edge magnetoplasmon in the presence of the drift velocity using the Wiener-Hopf method. We show that in the low-frequency and long-wavelength limit, v_{dr} provides additive contribution to the edge magnetoplasmon velocity, which agrees with traditional treatment [20,21] based on transition to a reference frame moving with the drift velocity v_{dr}. Our conclusion about additive contribution of the drift velocity holds both in the clean limit and in the presence of dissipation.

The presented analysis, where the Dirichlet boundary condition is imposed on electron wave functions, corresponds to a thin-film or 2D material with an abrupt edge, examples are etched semiconductor quantum wells, atomically thin transition metal dichalcogenides [47], and other 2D conducting and semiconducting materials such as phosphorene [48] or TiN [49]. The drift velocity of edge magnetoplasmons in such physical realizations with the hard edge has, to our knowledge, not been considered theoretically so far. Nevertheless, in the classical limit our results come to surprising agreement with the opposite picture of smooth edge created by confining electric field.

Out theoretical analysis opens the door for prediction of edge-mode velocities, taking into account the local edge response beyond long-wavelength phenomenological and classical approaches. Numerical calculations for specific physical realizations will be performed in the future. Further development of the theory adapted to more complicated electronic structure and electromagnetic response near the edge should take into account the appearance of dissipation at noninteger Landau-level fillings [31,34] and spatial structure of compressible and incompressible stripes [8,35]. Anisotropy of electron dispersion arising due to intrinsic properties of a material (such as AlAs [50]) or fabrication-related strain can also affect the edge state and edge magnetoplasmon physics. After a rescaling of coordinates, the anisotropy of effective mass becomes equivalent to anisotropic Coulomb interaction, which affects integer and fractional quantum Hall effects [50–53], uncovering the physics of electron nematics [54]. Edge-mode electrodynamics becomes more mathematically involved in the anisotropic case [42], so interplay of drift velocity and anisotropy deserves additional study. Multiple-subband effects can modify the structure of Landau levels triggering their crossing [55,56], and spin-orbit interaction arising at the interfaces where 2DEG is formed [57,58] can also modify the structure of Landau levels in the bulk [59,60] and near the edge [61]. These effects can change the edge magnetoplasmon properties and electromagnetic response of magnetic edge channels at specific Landau-level filling factors, however, we expect the qualitative features of drift velocity to be robust against band-structure modifications at low energy scale, because our results demonstrate correct quasiclassical limiting behavior arising when a large number of Landau levels is occupied.

It is also of interest to extend our theory on massless Dirac electrons in doped graphene, accounting for the specific character of their edge states at the boundaries of graphene lattice having different orientations [62], and on different unconventional materials such as quantum anomalous Hall insulators [26–28], magic-angle twisted bilayer graphene [63] with a flat-band electron spectrum, and other graphene-based heterostructures.

APPENDIX: QUASICLASSICAL APPROXIMATION FOR DRIFT VELOCITY

The problem (1) of one-dimensional motion in harmonic potential with hard wall

$$V(x) = \begin{cases} \frac{1}{2}m\omega_{\mathrm{c}}^2\left(x + l_H^2 k_y\right)^2, & x > 0 \\ +\infty, & x \leqslant 0 \end{cases} \quad \text{(A1)}$$

can be solved (see also Ref. [46]) in the quasiclassical approximation using the Einstein-Brillouin-Keller quantization condition [64]

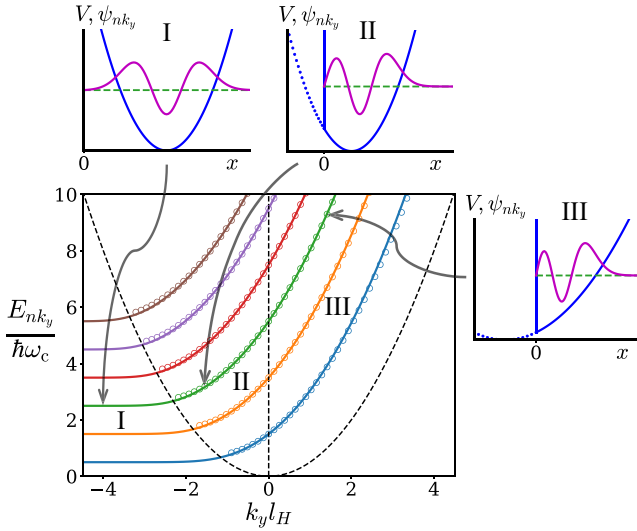$$\int_{x_1}^{x_2} p(x)\, dx = \pi\hbar(n + \alpha), \quad \text{(A2)}$$

FIG. 7. Exact energies of the edge states E_{nk_y} in magnetic field (solid lines) as functions of k_y, and their quasiclassical approximations (circles) given by Eq. (A6). Insets show quadratic confining potential $V(x)$ and wave function $\psi_{nk_y}(x)$ for $n=2$ in different regions of quasiclassical quantization.

where $E_{nk_y}^{\text{qc}}$ is the quasiclassical energy level, $p(x) = \{2m[E_{nk_y}^{\text{qc}} - V(x)]\}^{1/2}$, and the sum of Morse-Maslov indices α equals $\frac{1}{2}$ if the potential $V(x)$ is smooth at both turning points $x_{1,2}$, or $\frac{3}{4}$ if one of these points is located at the hard wall $x=0$.

Depending on $E_{nk_y}^{\text{qc}}$ and k_y, we identify different regimes of quasiclassical quantization shown in the insets of Fig. 7. At $k_y < -(2mE_{nk_y}^{\text{qc}})^{1/2}\hbar^{-1}$ (region I), both turning points lie at the parabolic part of $V(x)$, so we obtain $\int_{x_1}^{x_2} p(x)dx = \pi E_{nk_y}^{\text{qc}}/\omega_c$ and hence the familiar harmonic oscillator quasiclassical energies $E_{nk_y}^{\text{qc}} = \hbar\omega_c(n+\frac{1}{2})$ coinciding with the exact ones. At $-(2mE_{nk_y}^{\text{qc}})^{1/2}\hbar^{-1} < k_y < 0$ (region II) and $k_y > 0$ (region III), one of the turning points is the hard wall $x_1 = 0$, and the quantization condition (A2) reads

$$\frac{r(x)}{x} = \frac{n+\frac{3}{4}}{\varepsilon}, \tag{A3}$$

where $x = \varepsilon/z$, $\varepsilon = E_{nk_y}^{\text{qc}}/\hbar\omega_c$ is the dimensionless energy, and $z = l_H^2 k_y^2/2$. The function

$$r(x) = \frac{x}{2} - \text{sgn}(k_y)\left(\frac{x}{2} + \frac{\sqrt{x-1} - x\arctan\sqrt{x-1}}{\pi}\right) \tag{A4}$$

can be surprisingly well approximated by the simpler expression:

$$r(x) \approx \frac{x}{2} - \text{sgn}(k_y)\sqrt{\frac{4(x-1)}{\pi^2} + \frac{1}{4}}. \tag{A5}$$

From Eqs. (A3) and (A5), we can obtain the approximate quasiclassical energies in regions II and III,

$$E_{nk_y}^{\text{qc}} = \frac{4\hbar^2 k_y^2}{\pi^2 m} + \hbar\omega_c\left(2n+\frac{3}{2}\right) + \frac{2\sqrt{2}\hbar^2 k_y}{ml_H}\sqrt{2n+\frac{3}{2}+\frac{l_H^2 k_y^2}{2}\left(\frac{2}{\pi}-\frac{\pi}{4}\right)^2}, \tag{A6}$$

which are quite close to the exact ones, as shown in Fig. 7.

Using the quasiclassical dispersion equation (A2) and the property $xr'(x) - r(x) = \text{sgn}(k_y)\sqrt{x-1}/\pi$ of the exact function (A4), we obtain the derivative

$$\frac{\partial k_y}{\partial E_{nk_y}^{\text{qc}}} = \frac{\pi}{\hbar\omega_c l_H^2 |k_y|}\frac{r'(x)}{\sqrt{x-1}}, \tag{A7}$$

taken at $n = \text{const}$. If the equilibrium Fermi level E_F is located between n_0th and (n_0+1)th bulk Landau levels, and $n_0 \gg 1$ (as assumed in the quasiclassical limit), then we can approximate summation over n in Eq. (20) by continuous integration. Using Eq. (A7) and taking the quantization condition (A3) at $\varepsilon = \text{const}$ to switch from n to x, we obtain

$$\sum_{n=0}^{n_0}\frac{\partial k_n^{\max}}{\partial E_{nk_y}} \approx \frac{\pi}{\sqrt{2}\hbar\omega_c l_H}\int_0^{n_0} dn\sqrt{\frac{x}{\varepsilon}}\frac{r'(x)}{\sqrt{x-1}}$$
$$= \frac{1}{\sqrt{2}\hbar\omega_c l_H}\int_1^\infty \frac{dx}{x^{3/2}}\sqrt{\varepsilon} = \frac{1}{\hbar\omega_c l_H}\sqrt{\frac{2E_F}{\hbar\omega_c}}. \tag{A8}$$

Substituting this result to Eq. (20) and taking into account that $E_F \approx \hbar\omega_c(n_0+1)$, we obtain the final quasiclassical expression (44) for the drift velocity.

[1] A. L. Fetter, Edge magnetoplasmons in a bounded two-dimensional electron fluid, Phys. Rev. B **32**, 7676 (1985).

[2] N. Hiyama, M. Hashisaka, and T. Fujisawa, An edge-magnetoplasmon Mach-Zehnder interferometer, Appl. Phys. Lett. **107**, 143101 (2015).

[3] M. Hashisaka, H. Kamata, N. Kumada, K. Washio, R. Murata, K. Muraki, and T. Fujisawa, Distributed-element circuit model of edge magnetoplasmon transport, Phys. Rev. B **88**, 235409 (2013).

[4] D. Jin, L. Lu, Z. Wang, C. Fang, J. D. Joannopoulos, M. Soljačić, L. Fu, and N. X. Fang, Topological magnetoplasmon, Nat. Commun. **7**, 13486 (2016).

[5] A. C. Mahoney, J. I. Colless, S. J. Pauka, J. M. Hornibrook, J. D. Watson, G. C. Gardner, M. J. Manfra, A. C. Doherty, and D. J. Reilly, On-chip microwave quantum Hall circulator, Phys. Rev. X **7**, 011007 (2017).

[6] M. Wassermeier, J. Oshinowo, J. P. Kotthaus, A. H. MacDonald, C. T. Foxon, and J. J. Harris, Edge magnetoplasmons in the fractional-quantum-Hall-effect regime, Phys. Rev. B **41**, 10287 (1990).

[7] R. C. Ashoori, H. L. Stormer, L. N. Pfeiffer, K. W. Baldwin, and K. West, Edge magnetoplasmons in the time domain, Phys. Rev. B **45**, 3894 (1992).

[8] V. I. Talyanskii, A. V. Polisski, D. D. Arnone, M. Pepper, C. G. Smith, D. A. Ritchie, J. E. Frost, and G. A. C.

Jones, Spectroscopy of a two-dimensional electron gas in the quantum-Hall-effect regime by use of low-frequency edge magnetoplasmons, Phys. Rev. B **46**, 12427 (1992).

[9] G. Ernst, N. B. Zhitenev, R. J. Haug, and K. von Klitzing, Dynamic excitations of fractional quantum Hall edge channels, Phys. Rev. Lett. **79**, 3748 (1997).

[10] D. B. Mast, A. J. Dahm, and A. L. Fetter, Observation of bulk and edge magnetoplasmons in a two-dimensional electron fluid, Phys. Rev. Lett. **54**, 1706 (1985).

[11] V. I. Talyanskii, M. Y. Simmons, J. E. F. Frost, M. Pepper, D. A. Ritchie, A. C. Churchill, and G. A. C. Jones, Experimental investigation of the damping of low-frequency edge magnetoplasmons in GaAs-Al$_x$Ga$_{1-x}$As heterostructures, Phys. Rev. B **50**, 1582 (1994).

[12] H. Kamata, T. Ota, K. Muraki, and T. Fujisawa, Voltage-controlled group velocity of edge magnetoplasmon in the quantum Hall regime, Phys. Rev. B **81**, 085329 (2010).

[13] N. Kumada, H. Kamata, and T. Fujisawa, Edge magnetoplasmon transport in gated and ungated quantum Hall systems, Phys. Rev. B **84**, 045314 (2011).

[14] I. V. Andreev, V. M. Muravev, D. V. Smetnev, and I. V. Kukushkin, Acoustic magnetoplasmons in a two-dimensional electron system with a smooth edge, Phys. Rev. B **86**, 125315 (2012).

[15] A. Endo, K. Koike, S. Katsumoto, and Y. Iye, Frequencies of the edge-magnetoplasmon excitations in gated quantum Hall edges, J. Phys. Soc. Jpn. **87**, 064709 (2018).

[16] J. Wu, O. Sydoruk, A. S. Mayorov, C. D. Wood, D. Mistry, L. Li, E. H. Linfield, A. Giles Davies, and J. E. Cunningham, Time-domain measurement of terahertz frequency magnetoplasmon resonances in a two-dimensional electron system by the direct injection of picosecond pulsed currents, Appl. Phys. Lett. **108**, 091109 (2016).

[17] N. Kumada, N.-H. Tu, K.-i. Sasaki, T. Ota, M. Hashisaka, S. Sasaki, K. Onomitsu, and K. Muraki, Suppression of gate screening on edge magnetoplasmons by highly resistive ZnO gate, Phys. Rev. B **101**, 205205 (2020).

[18] I. Crassee, M. Orlita, M. Potemski, A. L. Walter, M. Ostler, T. Seyller, I. Gaponenko, J. Chen, and A. B. Kuzmenko, Intrinsic terahertz plasmons and magnetoplasmons in large scale monolayer graphene, Nano Lett. **12**, 2470 (2012).

[19] H. Yan, Z. Li, X. Li, W. Zhu, P. Avouris, and F. Xia, Infrared spectroscopy of tunable Dirac terahertz magneto-plasmons in graphene, Nano Lett. **12**, 3766 (2012).

[20] N. Kumada, S. Tanabe, H. Hibino, H. Kamata, M. Hashisaka, K. Muraki, and T. Fujisawa, Plasmon transport in graphene investigated by time-resolved electrical measurements, Nat. Commun. **4**, 1363 (2013).

[21] N. Kumada, P. Roulleau, B. Roche, M. Hashisaka, H. Hibino, I. Petković, and D. C. Glattli, Resonant edge magnetoplasmons and their decay in graphene, Phys. Rev. Lett. **113**, 266601 (2014).

[22] I. Petković, F. I. B. Williams, K. Bennaceur, F. Portier, P. Roche, and D. C. Glattli, Carrier drift velocity and edge magnetoplasmons in graphene, Phys. Rev. Lett. **110**, 016801 (2013).

[23] X. Lin, Y. Xu, B. Zhang, R. Hao, H. Chen, and E. Li, Unidirectional surface plasmons in nonreciprocal graphene, New J. Phys. **15**, 113003 (2013).

[24] I. Petković, F. I. B. Williams, and D. C. Glattli, Edge magnetoplasmons in graphene, J. Phys. D **47**, 094010 (2014).

[25] N. Kumada, R. Dubourget, K. Sasaki, S. Tanabe, H. Hibino, H. Kamata, M. Hashisaka, K. Muraki, and T. Fujisawa, Plasmon transport and its guiding in graphene, New J. Phys. **16**, 063055 (2014).

[26] A. C. Mahoney, J. I. Colless, L. Peeters, S. J. Pauka, E. J. Fox, X. Kou, L. Pan, K. L. Wang, D. Goldhaber-Gordon, and D. J. Reilly, Zero-field edge plasmons in a magnetic topological insulator, Nat. Commun. **8**, 1836 (2017).

[27] T. Wang, C. Wu, M. Mogi, M. Kawamura, Y. Tokura, Z.-X. Shen, Y.-Z. You, and M. T. Allen, Probing the edge states of Chern insulators using microwave impedance microscopy, Phys. Rev. B **108**, 235432 (2023).

[28] L. A. Martinez, G. Qiu, P. Deng, P. Zhang, K. G. Ray, L. Tai, M.-T. Wei, H. He, K. L. Wang, J. L. DuBois, and D.-X. Qu, Edge magnetoplasmon dispersion and time-resolved plasmon transport in a quantum anomalous Hall insulator, Phys. Rev. Res. **6**, 013081 (2024).

[29] W. Wang, J. M. Kinaret, and S. P. Apell, Excitation of edge magnetoplasmons in semi-infinite graphene sheets: Temperature effects, Phys. Rev. B **85**, 235444 (2012).

[30] I. L. Aleiner and L. I. Glazman, Novel edge excitations of two-dimensional electron liquid in a magnetic field, Phys. Rev. Lett. **72**, 2935 (1994).

[31] M. D. Johnson and G. Vignale, Dynamics of dissipative quantum Hall edges, Phys. Rev. B **67**, 205332 (2003).

[32] V. A. Volkov and S. A. Mikhailov, Edge magnetoplasmons: Low frequency weakly damped excitations in inhomogeneous two-dimensional electron systems, Zh. Eksp. Teor. Fiz. **94**, 217 (1988) [Sov. Phys. JETP **67**, 1639 (1988)].

[33] D. Margetis, Edge plasmon-polaritons on isotropic semi-infinite conducting sheets, J. Math. Phys. **61**, 062901 (2020).

[34] A. A. Sokolik and Y. E. Lozovik, Edge magnetoplasmons in graphene: Effects of gate screening and dissipation, Phys. Rev. B **100**, 125409 (2019).

[35] D. B. Chklovskii, B. I. Shklovskii, and L. I. Glazman, Electrostatics of edge channels, Phys. Rev. B **46**, 4026 (1992).

[36] O. G. Balev and P. Vasilopoulos, Edge magnetoplasmons for very low temperatures and sharp density profiles, Phys. Rev. B **56**, 13252 (1997).

[37] O. G. Balev, P. Vasilopoulos, and H. O. Frota, Edge magnetoplasmons in wide armchair graphene ribbons, Phys. Rev. B **84**, 245406 (2011).

[38] G. Sukhodub, F. Hohls, and R. J. Haug, Observation of an interedge magnetoplasmon mode in a degenerate two-dimensional electron gas, Phys. Rev. Lett. **93**, 196801 (2004).

[39] B. I. Halperin, Quantized Hall conductance, current-carrying edge states, and the existence of extended states in a two-dimensional disordered potential, Phys. Rev. B **25**, 2185 (1982).

[40] P. Dean, The constrained quantum mechanical harmonic oscillator, Math. Proc. Cambridge Philos. Soc. **62**, 277 (1966).

[41] L. Landau and E. Lifshitz, *Quantum Mechanics: Non-Relativistic Theory*, Vol. 3 (3rd ed.) (Pergamon Press, Oxford, 1977).

[42] A. A. Sokolik, O. V. Kotov, and Y. E. Lozovik, Plasmonic modes at inclined edges of anisotropic two-dimensional materials, Phys. Rev. B **103**, 155402 (2021).

[43] D. Margetis, M. Maier, T. Stauber, T. Low, and M. Luskin, Nonretarded edge plasmon-polaritons in anisotropic two-dimensional materials, J. Phys. A: Math. Theor. **53**, 055201 (2020).

[44] G. Carrier, M. Krook, and C. Pearson, *Functions of a Complex Variable: Theory and Technique* (SIAM, Philadelphia, 2005).

[45] E. Nikulin, D. Mylnikov, D. Bandurin, and D. Svintsov, Edge diffraction, plasmon launching, and universal absorption enhancement in two-dimensional junctions, Phys. Rev. B **103**, 085306 (2021).

[46] G. Montambaux, Semiclassical quantization of skipping orbits, Eur. Phys. J. B **79**, 215 (2011).

[47] G. Wang, A. Chernikov, M. M. Glazov, T. F. Heinz, X. Marie, T. Amand, and B. Urbaszek, Colloquium: Excitons in atomically thin transition metal dichalcogenides, Rev. Mod. Phys. **90**, 021001 (2018).

[48] R. Y. Kezerashvili, A. Spiridonova, and A. Dublin, Magnetoexcitons in phosphorene monolayers, bilayers, and van der Waals heterostructures, Phys. Rev. Res. **4**, 013154 (2022).

[49] D. Shah, M. Yang, Z. Kudyshev, X. Xu, V. M. Shalaev, I. V. Bondarev, and A. Boltasseva, Thickness-dependent Drude plasma frequency in transdimensional plasmonic tin, Nano Lett. **22**, 4622 (2022).

[50] M. Shayegan, E. P. De Poortere, O. Gunawan, Y. P. Shkolnikov, E. Tutuc, and K. Vakili, Two-dimensional electrons occupying multiple valleys in AlAs, Phys. Status Solidi (b) **243**, 3629 (2006).

[51] D. B. Balagurov and Y. E. Lozovik, Fermi surface of composite fermions and one-particle excitations at $\nu = \frac{1}{2}$: Effect of band-mass anisotropy, Phys. Rev. B **62**, 1481 (2000).

[52] O. Ciftja, Integer quantum Hall effect with an anisotropic Coulomb interaction potential, J. Phys. Chem. Solids **156**, 110131 (2021).

[53] N. Jiang, S. Ke, H. Ji, H. Wang, Z.-X. Hu, and X. Wan, Principal component analysis of the geometry in anisotropic quantum Hall states, Phys. Rev. B **102**, 115140 (2020).

[54] E. Fradkin, S. A. Kivelson, M. J. Lawler, J. P. Eisenstein, and A. P. Mackenzie, Nematic Fermi fluids in condensed matter physics, Annu. Rev. Condens. Matter Phys. **1**, 153 (2010).

[55] X. C. Zhang, D. R. Faulhaber, and H. W. Jiang, Multiple phases with the same quantized Hall conductance in a two-subband system, Phys. Rev. Lett. **95**, 216801 (2005).

[56] C. Ellenberger, B. Simovič, R. Leturcq, T. Ihn, S. E. Ulloa, K. Ensslin, D. C. Driscoll, and A. C. Gossard, Two-subband quantum Hall effect in parabolic quantum wells, Phys. Rev. B **74**, 195313 (2006).

[57] G. Khalsa, B. Lee, and A. H. MacDonald, Theory of t_{2g} electron-gas Rashba interactions, Phys. Rev. B **88**, 041302(R) (2013).

[58] J. Zhou, W.-Y. Shan, and D. Xiao, Spin responses and effective Hamiltonian for the two-dimensional electron gas at the oxide interface $LaAlO_3/SrTiO_3$, Phys. Rev. B **91**, 241302(R) (2015).

[59] X. F. Wang and P. Vasilopoulos, Magnetotransport in a two-dimensional electron gas in the presence of spin-orbit interaction, Phys. Rev. B **67**, 085313 (2003).

[60] D. Zhang, Exact Landau levels in two-dimensional electron systems with Rashba and Dresselhaus spin–orbit interactions in a perpendicular magnetic field, J. Phys. A: Math. Gen. **39**, L477 (2006).

[61] V. L. Grigoryan, A. Matos Abiague, and S. M. Badalyan, Spin edge states: An exact solution and oscillations of the spin current, Phys. Rev. B **80**, 165320 (2009).

[62] D. A. Abanin, P. A. Lee, and L. S. Levitov, Charge and spin transport at the quantum Hall edge of graphene, Solid State Commun. **143**, 77 (2007).

[63] T.-N. Do, P.-H. Shih, and G. Gumbs, Magnetoplasmons in magic-angle twisted bilayer graphene, J. Phys.: Condens. Matter **35**, 455703 (2023).

[64] M. Brack and R. Bhaduri, *Semiclassical Physics* (CRC Press, Boca Raton, 2003), 1st ed.